IEEE Access
Multidisciplinary | Rapid Review | Open Access Journal

SPECIAL SECTION ON WEARABLE AND IMPLANTABLE DEVICES AND SYSTEMS

Received March 23, 2018, accepted May 10, 2018, date of publication May 25, 2018, date of current version June 20, 2018.

Digital Object Identifier 10.1109/ACCESS.2018.2840689

Integrated Design of Wideband Omnidirectional Antenna and Electronic Components for Wireless Capsule Endoscopy Systems

ZHU DUAN[1], (Member, IEEE), LI-JIE XU[2], (Member, IEEE), STEVEN GAO[3], (Senior Member, IEEE), AND WEN GEYI[1], (Member, IEEE)

[1]Research Center of Applied Electromagnetics, Nanjing University of Information Science and Technology, Nanjing 210044, China
[2]National and Local Joint Engineering Laboratory of RF Integration and Micro-Assembly Technology, Nanjing University of Posts and Telecommunications, Nanjing 210023, China
[3]School of Engineering and Digital Arts, University of Kent, Canterbury CT2 7NZ, U.K.

Corresponding author: Steven Gao (s.gao@kent.ac.uk)

This work was supported in part by the Natural Science Foundation of Jiangsu Province under Grants BK20170957 and BK20160917, in part by the Startup Foundation for Introducing Talent of NUIST, in part by the National Natural Science Foundation of China under Grant 61601241, and in part by the Priority Academic Program Development of Jiangsu Higher Education Institutions.

ABSTRACT This paper presents a wideband antenna with omnidirectional radiation pattern for wireless capsule endoscopy (WCE) systems. The proposed antenna radiates as slot structure formed between a central copper cylinder and a copper strip attached to the interior surface of biocompatible polyimide shell. Main features of the antenna include: 1) an integrated design of the antenna and electronic components in the capsule is employed. And by utilizing the entire inner space of the capsule, the radiating aperture of antenna is increased to the maximum; 2) the copper cylinder can be used to house electronic components, therefore the potential electromagnetic interferences brought by battery and electronic circuits are reduced to the minimum; 3) the antenna in tissue has a wide bandwidth from 0.721 to 1.705 GHz, covering both 0.902–0.928-GHz industrial, scientific, and medical band and 1.395–1.4-GHz wireless medical telemetry service band; and 4) the antenna inside human tissues has stable omnidirectional radiation patterns across all operating frequencies. This is an indispensable characteristic due to unpredictable orientation of the capsule in gastrointestinal tract. The integrated design concept, wideband impedance matching, and stable omnidirectional radiation patterns make the proposed antenna a promising candidate for future WCE system.

INDEX TERMS Wireless capsule antenna, integrated design, wideband, ISM band, WMTS band, omnidirectional radiation pattern.

I. INTRODUCTION

Improvement of human health is the key aim of scientific research, and novel products integrated with latest technology for health care and medical diagnosis are in urgent demand. During recent years, rapid development in both electronic and biomedical technology helps motivate professionals to come up with many interdisciplinary ideas, and wireless capsule endoscopy (WCE) system is one of them. Due to its noninvasive nature during the process of recording physiological data and delivering images along gastrointestinal (GI) tract, this WCE technology attracts attention from both industrial and academic communities [1], [2].

Various types of antenna for endoscopy have been proposed. For instance, spiral antennas are proposed operating at 500 MHz with isotropic radiation pattern [3], [4]. Meandered dipole antennas are proposed to reduce the antenna size operating at WMTS and ISM bands [5]–[7]. Microstrip antenna with half-wave stepped-impedance resonator technique for matching purpose is also presented [8]. Loop antennas with better conformal capabilities are proposed with wide bandwidth achieved [9], [10].

In addition to these linearly polarized antennas, a circularly polarized (CP) helical antenna operating at 2.4-2.48 GHz ISM band is proposed with an axial ratio (AR) bandwidth of 33.3% [11]. Another CP antenna operating at 915 MHz ISM band is presented with a 3-dB AR bandwidth of around 29.2% [12]. Besides of these CP antennas, a more recent work proposes an orientation insensitive antenna with polarization

diversity by using three orthogonal currents [13]. In addition, our previous work proposed a dual band mixed-polarization capsule antenna, with linearly polarized property at 1.4 GHz WMTS band, and circularly polarized property at 2.45 GHz ISM band [14].

These past research works have presented interesting ideas in designing capsule antenna. However, with the additional battery and electronic circuits embedded in the capsule device, the antenna performance will be degraded due to the electronic components' electromagnetic interference (EMI). For instance, the antenna gain is reduced from −19.4 to −25.2 dBi for the case shown in [12]. Even if the EMI issue is considered [15], [16], the proposed patch antenna's bandwidth (around 11% in [15], around 8% in [16]) is not wide enough to withstand the frequency shift in the real-world tissue environment. Therefore, this paper starts the antenna design by taking into account of the electronic components and antenna together.

Compared with past research works, the proposed antenna has several unique features:

1) An integrated design of the antenna and electronic components in the capsule is employed. Slot structure is formed between a central copper cylinder and a copper strip attached to the interior surface of the biocompatible polyimide shell. In this way, the entire inner space of the capsule is utilized to maximize the radiating aperture, which helps increase the antenna's gain-bandwidth product [17]–[19]. In addition, a slot antenna can be regarded as a magnetic source, which radiates more efficiently than electrical antennas when implanted into lossy tissues [20].
2) Electronic components are considered at the start of antenna design. A copper cylinder, which can be made hollow to house the battery and other electronic circuits, is introduced within the antenna, therefore minimizing the EMI brought by them. Besides, this copper cylinder also takes part in radiation, which further helps maximize the antenna's gain-bandwidth product.
3) The antenna has a wide impedance bandwidth from 0.721 to 1.705 GHz. This is partially achieved by optimizing the stepped width of copper strip along the interior surface of biocompatible polyimide shell.
4) The antenna has stable omnidirectional radiation patterns across all operating frequencies within the impedance bandwidth. This is achieved by forming strong electric fields within the top substrate, pointing towards the same direction. Due to the capsule's unpredictable orientation in GI tract, this characteristic helps ensure robust communication between internal capsule antenna and external wearable repeater devices [21]–[24] or monitoring console.

II. ANTENNA DESIGN

It is important to take into account of all electronic and optical components while designing the capsule antenna. Normally, a wireless capsule endoscopy system is comprised of biocompatible shell, an optical dome, light-emitting diode (LED), camera, battery, transmitter circuits and antenna [4], [6]. The optical dome should be made transparent for the LED to shed light on the internal tissue, and then the camera can take pictures and sensors can record physiological data; afterwards, the digitized information is sent to the circuits for processing; finally, the data can be further transmitted to external device by antenna. The simplified schematic for the WCE system and its application in human's GI tract are shown in Fig. 1.

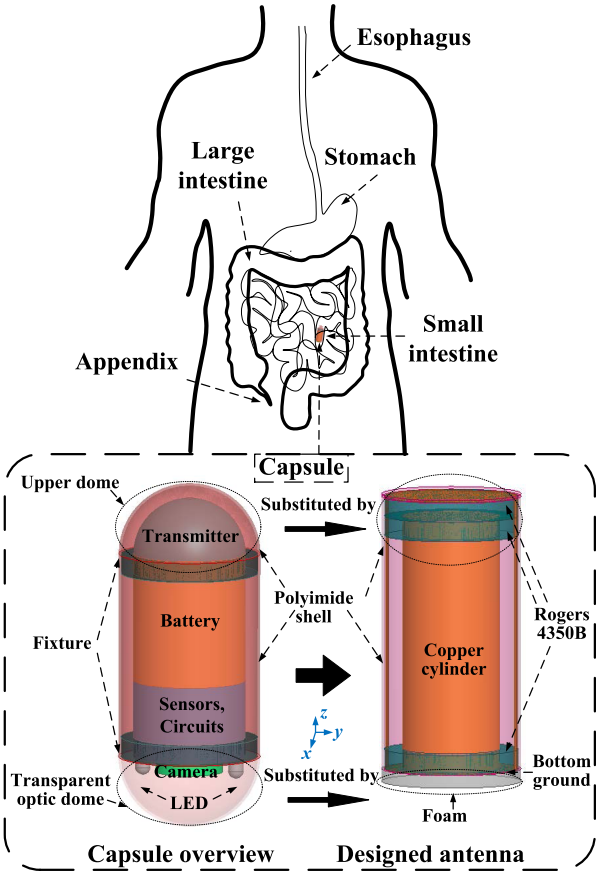

FIGURE 1. Simplified schematic for wireless capsule endoscopy system and its application in gastrointestinal tract.

A. ANTENNA STRUCTURE

As can be seen from Fig.1, in order to ensure manufacture and assembly precision for our proposed antenna, the upper dome of the capsule has been substituted by a short cylindrical structure and the lower optic dome has been substituted by cylinder shaped foam. To get a clearer view of the proposed antenna, its exploded view together with its front, top and side views is shown in Fig. 2. The foam is added just to isolate the conducting effect of surrounding tissue, and its thickness has little influence on antenna performance, which will be validated in Section III. Considering the EMI of electronic components, a copper cylinder is introduced in the center, and the upper portion of the cylinder can be

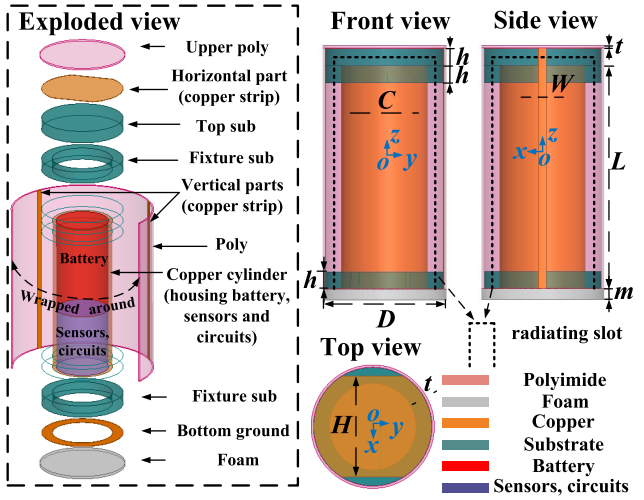

FIGURE 2. Exploded view of proposed antenna and its front, side and top views.

made hollow to house the transmitter circuits while the lower portion can be used to house battery, sensors and other electronic components. Along the interior surface of polyimide shell, copper strip with stepped width is introduced, which is composed of a wide horizontal part on top and two vertical parts symmetrically placed at two sides of the shell. Furthermore, another horizontal copper plane is introduced at the bottom, connected to both the copper cylinder and the vertical strip parts at two sides. For the fixture or spacer, two Rogers 4350B substrates are adopted encircling the copper cylinder, with an additional Rogers 4350B substrate positioned at the top to support the horizontal strip part. With the antenna implemented in this way, half wavelength resonant slot can be successfully excited, and all the electronic components can be placed inside the copper cylinder and therefore cause little influence on the slot antenna's matching and radiation performance. The proposed antenna's geometry is symmetric with respect to both *xoz* and *yoz* planes and the antenna size is 11 mm (D, Diameter) × 22 mm (L_g, Length). As for the antenna's geometric parameters, which are listed in Table 1, are optimized by Ansys High Frequency Structural Simulator (HFSS).

TABLE 1. Antenna's geometric parameters.

Symbol	Value (mm)	Symbol	Value (mm)
L	20.0	W	0.6
C	8.0	D	11.0
h	1.524	t	0.07
m	0.336	H	9.0

B. ANTENNA PERFORMANCE

In simulation, the antenna is placed in the center of a cylindrical muscle tissue with a size of 110 mm (D_t, Diameter) × 80 mm (D_p, Deepness). The muscle tissue is set to be frequency dependent according to [25], and the typical dielectric properties at 0.915 GHz and 1.4 GHz are $\varepsilon_r = 54.99$, $\sigma = 0.948$ S/m and $\varepsilon_r = 54.11$, $\sigma = 1.142$ S/m respectively. For the antenna feeding during simulation, one method is through a lumped port located in the center of the top substrate. This is similar to actual application where the antenna is directly connected to the output of circuits, but not easily realizable during measurement. Another method is through a wave port at the bottom of a coaxial cable connected with the antenna, which is similar to our measurement setup. The simplified schematic for simulation setup together with two feeding methods is shown in Fig. 3(a), and the comparison of reflection coefficients for these two feeding methods is shown in Fig. 3(b).

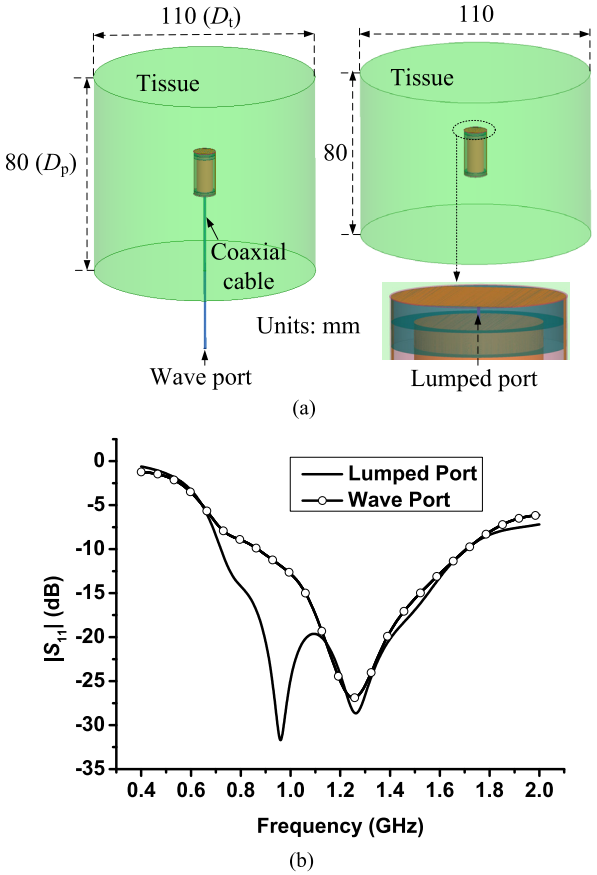

FIGURE 3. (a) Simplified schematic for simulation setup with two feeding methods. (b) Comparison of reflection coefficients for two feeding methods.

From Fig. 3(b) we can see that the antenna's bandwidth fed by lumped port is very large, which spans from 0.721 to 1.705 GHz. This wideband characteristic is attributed to two factors: 1) the entire inner space of the capsule is utilized to achieve a maximum radiation aperture, therefore maximizing the gain-bandwidth product; 2) through the variation of W (width of vertical strip parts) and H (width of horizontal strip part), the capacitance formed between the copper cylinder and the copper strip can be easily tuned, resulting in a wideband performance.

For the case of wave port feeding (cable length: 100 mm), the antenna bandwidth is reduced to 840 MHz

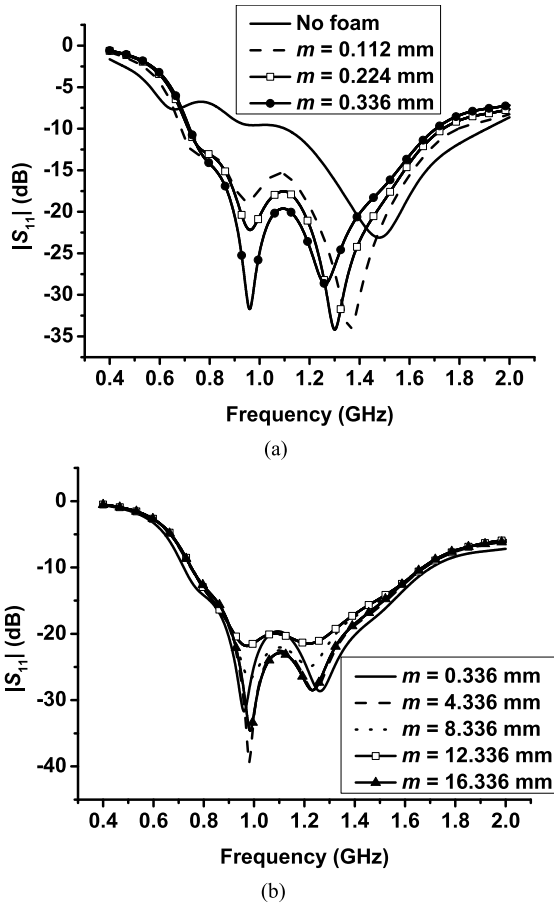

FIGURE 4. (a) Comparison of reflection coefficients with *m* varied from 0 to 0.336 mm. (b) Comparison of reflection coefficients with *m* varied from 0.336 to 16.336 mm.

(0.868 to 1.708 GHz) compared with 984 MHz for the lumped port case. However, the wideband characteristic is still maintained, validating the stability of our proposed structure. The bandwidth reduction is mainly caused by the alteration of extended cable's surface current due to the loading of lossy tissue, and the effect of feeding cable will be elaborated in Section III. Besides, for all simulations performed in following context, lumped port is used as the default one.

III. ANTENNA SIMULATION

A. FOAM THICKNESS

The foam, which is used to substitute the transparent optic dome in the capsule prototype, is added to isolate the conducting effect of tissue. To view the loading effect of foam, it is removed at first, and then its thickness (m) is gradually increased to 0.366 mm at a step of 0.112 mm. As shown in Fig. 4(a), the antenna with no foam loaded has a resonant frequency of 1.48 GHz. When the bottom ground plane is separated by foam even with a small thickness ($m = 0.112$ mm), the antenna's matching at 0.902-0.928 GHz ISM band is greatly improved. With m further increased to 0.336 mm, the antenna achieves a decent matching performance at desired ISM and WMTS bands.

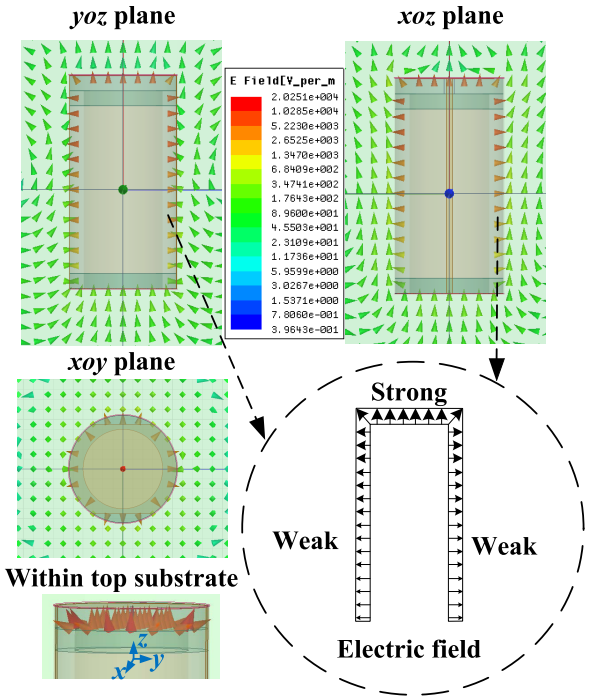

FIGURE 5. Electric field distributions at 1.48 GHz for three orthogonal planes with an input power of 1 W.

If we increase m further as shown in Fig. 4(b), the antenna's matching oscillates, nonetheless, the wide band characteristic covering both 0.902-0.928 GHz ISM band and 1.395-1.4 GHz WMTS band is maintained. Therefore we are confident that, with the additional loading of optic modules, our proposed antenna's matching performance can stay almost unaffected.

B. OPERATING PRINCIPLE

In order to understand the operating principle of proposed antenna, the antenna's electric field distributions (input power: 1 W) without foam loading at 1.48 GHz for three orthogonal planes are plotted in Fig. 5. From Fig. 5 we can notice that the field distributions of *xoz* and *yoz* plane are similar and the antenna radiates through half wavelength resonant slots with maximum electric field concentrated within the top substrate. As these electric field vectors all point at positive z-axis, it results in an omnidirectional radiation pattern on the *xoy* plane. Additionally, the slot maximally utilizes the capsule's aperture, resulting in a large gain-bandwidth product. From the field distribution on *xoy* plane we can see that uniform radial-shaped electric field is concentrated in the space between the external polyimide shell and the copper cylinder. This characteristic helps reduce the Specific Absorption Rate (SAR) concentration in tissue, which will be further expounded in Subsection G of this section.

Also we can notice that the complete slot is composed of two portions, one is vertical air portion between the shell and copper cylinder, the other is horizontal dielectric portion (Rogers 4350B) located at the top. The total slot

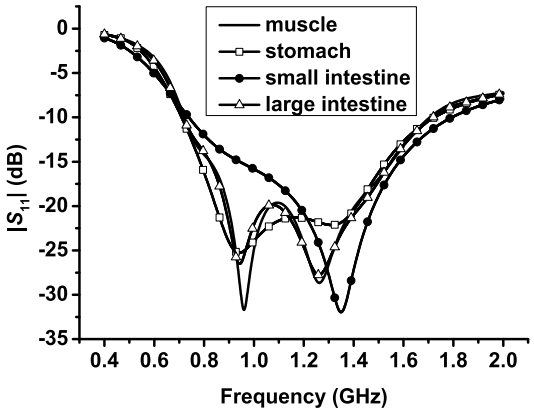

FIGURE 6. Comparison of reflection coefficients in four different tissues.

length in one orthogonal plane (either xoz or yoz plane) is around 51 mm ($\lambda_g/2$), approximately a quarter wavelength ($\lambda_0 = 300/1.48 = 203$ mm) at 1.48 GHz in air, attributed to the loading of surrounding tissue with high dielectric permittivity ($\varepsilon_r = 54 \sim 55$). Therefore, for this structure, the effective relative permittivity ε_{eff} for the combined air-tissue medium is around 4. Moreover, for actual application, the vertical air portion can be substituted by dielectric material, which not only helps reduce the overall capsule size, but also ensures the structural stability.

C. ANTENNA ROBUSTNESS

When the wireless capsule is swallowed by human, it will travel from esophagus to stomach, then to small intestine, further to large intestine and finally be evacuated. Therefore, the matching of the antenna in different tissues varies considerably. In order to evaluate the extent of matching variation, in addition to our original case in muscle, we put the antenna in three other tissues: stomach, small intestine and large intestine. All tissues are set to be frequency dependent according to [25], and the typical dielectric properties at 0.915 GHz for these three tissues are $\varepsilon_r = 65.02, \sigma = 1.193$ S/m, $\varepsilon_r = 59.39, \sigma = 2.173$ S/m and $\varepsilon_r = 57.87, \sigma = 1.087$ S/m respectively. The comparison of reflection coefficients in four tissues is presented in Fig. 6. From the figure we can see that our proposed antenna is very robust in various tissues, which make it a promising candidate of WCE system intended for GI tract imaging.

D. RADIATION PATTERN

The antenna's 3D radiation patterns at 0.915 GHz and 1.4 GHz are shown in Fig. 7(a) and the radiation patterns of *xoy* plane from 0.6 to 1.5 GHz at a step of 0.3 GHz are shown in Fig. 7(b). From the figure we can see that the proposed antenna can maintain a stable omnidirectional radiation pattern across all operating frequencies within the impedance bandwidth. The maximum gain values from 0.4 to 2 GHz at three directions are shown in Fig. 7(c). It can be noticed that three lines almost coincide with each other, and the maximum discrepancy between them is below 0.5 dB within our

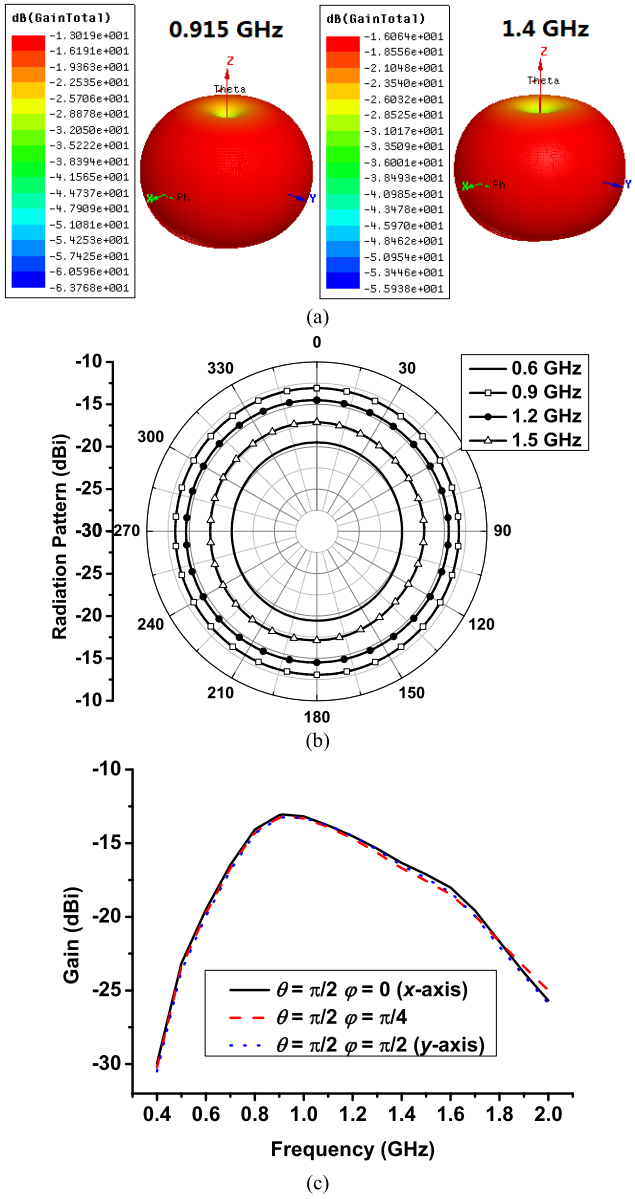

FIGURE 7. (a) 3D Radiation pattern at 0.915 GHz and 1.4 GHz, (b) radiation pattern of *xoy* plane from 0.6 to 1.5 GHz, (c) Gain values from 0.4 to 2 GHz.

proposed operating band (0.721 to 1.705 GHz). Considering the uncertainty of capsule orientation in human body, our proposed antenna's stable omnidirectional radiation pattern helps the WCE system build a robust telemetry with wearable device or monitoring console. In addition, the maximum gain (-13 dBi) is achieved around 0.915 GHz ISM band, and the frequency range where gain value exceeds -20 dBi spans from 0.6 to 1.69 GHz, which further validates our antenna's stable radiation performance.

E. TISSUE SIZE

From our past experience, as long as the tissue is not incredibly small, the tissue size won't affect the embedded antenna's reflection coefficient much [26], [27]. However, it does affect

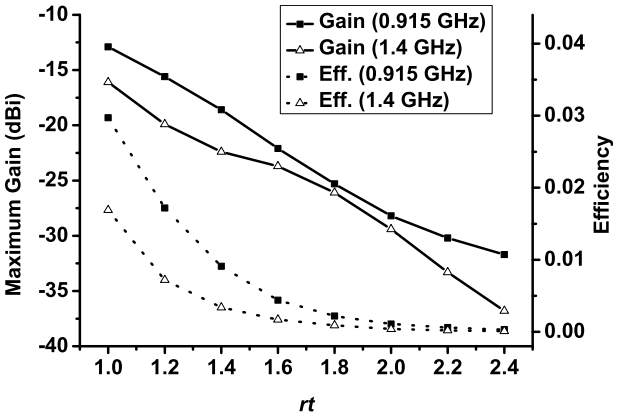

FIGURE 8. Maximum gain and radiation efficiency versus tissue size.

the gain and radiation efficiency, which is obvious because larger tissue with high tanδ brings more loss. Therefore when the antenna is surrounded by lossy tissue, without specifying the tissue size and the embedded location in the tissue, the value of antenna gain is meaningless. In our evaluation, we assume the original tissue's diameter D_t and deepness D_p are both multiplied by a ratio *rt*. With *rt* increased from 1 to 2.4 at a step of 0.2, the variation of radiation performance is shown in Fig. 8. For all cases, we put the antenna in the geometric center of the tissue. From the figure we can see that the antenna's maximum gain and radiation efficiency reduce rapidly with the increasing of tissue size. The detailed values of maximum gain and radiation efficiency at 0.915 GHz and 1.4 GHz for two tissue sizes are listed in Table 2.

TABLE 2. Antenna's radiation performance.

Tissue size ($D_t \times D_p$)	110 mm × 80 mm		220 mm × 160 mm	
Frequency	0.915 GHz	1.4 GHz	0.915 GHz	1.4 GHz
Maximum gain (dBi)	-13.0	-16.1	-28.2	-29.4
Radiation efficiency	2.97 %	1.69 %	0.11 %	0.04 %

F. EFFECT OF FEEDING CABLE

As stated in Subsection B of Section II, the antenna is evaluated with extended coaxial cable during measurement, and the additional cable embedded in tissue will influence the antenna's matching performance. In order to evaluate the influence, we assume four different locations where the wave port lies (*e* represents extended cable's length), and a copper pin is added in the center of the top substrate for feeding purpose.

Case a: with feeding pin only ($e = 0$ mm)

Case b: within the central copper cylinder ($0 < e < 20$ mm);

Case c: between the copper cylinder and tissue ($20 < e < 60$ mm);

Case d: outside the tissue ($e > 60$ mm).

The simplified schematic for four cases is shown in Fig. 9(a), and the tissue size is not in proportion for clearer

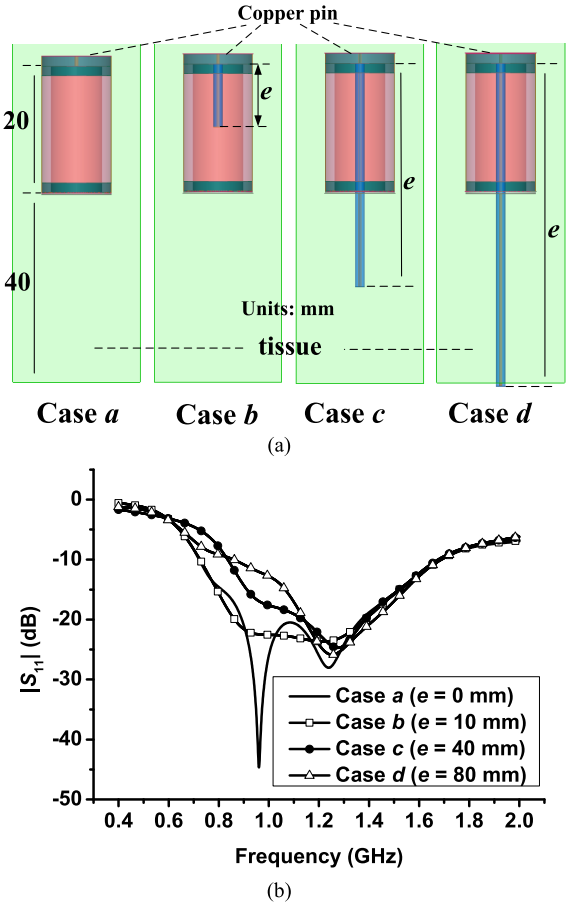

FIGURE 9. (a) Simplified schematic of four feeding cases (tissue size is not in proportion with antenna). (b) Comparison of simulated reflection coefficients with different lengths of feeding cable.

presentation. The comparison of reflection coefficients for these four cases is shown in Fig. 9(b). From the figure we can see that the curve of case *a* is quite similar with that of the default lumped port case shown in Fig. 3(b).

Moreover, if we perform a detailed parameter sweep of *e* in each case, we can find that when the port lies within the copper cylinder, the reflection coefficient stays almost unchanged thanks to the cylinder's shielding effect. Also, the $|S_{11}|$ curve of this case is similar to that of the lumped port case, and both cases are quite close to actual application. However, when the port is placed outside the copper cylinder, the cable's surface current is altered, which affects the antenna's matching performance. The influence of feeding cable has also been observed in [28]. Further, from Fig. 9(b) we can see that the effect on lower frequency band is more severe, which leads to narrower bandwidth compared with the original lumped port case. When the port lies in the area outside the tissue, the matching stays almost unaffected with further extension of the cable, due to the fact that the length of the cable interacting with tissue stays unchanged. The comparison of detailed parameter sweep of *e* is not presented for brevity.

G. SAR EVALUATION

Because the electromagnetic (EM) wave generated by capsule antenna propagates through human tissue, the temperature of the tissue surrounding WCE system will be raised. Normally, the energy absorbed by tissue is evaluated by SAR. SAR value (W/kg) at a certain point can be calculated by (1), where σ is tissue conductivity (S/m), ρ is tissue's mass density (kg/m^3) and E is the electric field strength in tissue (V/m) [29].

$$\mathrm{SAR} = \frac{\sigma\,|E|^2}{\rho} \tag{1}$$

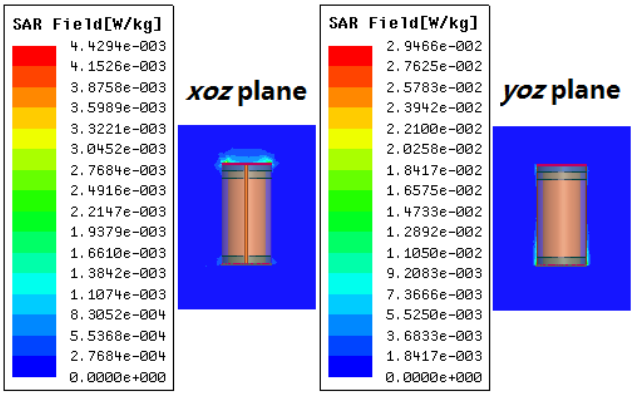

FIGURE 10. Local SAR distributions at 0.915 GHz.

For our design, the input power is set to be −25 dBm (3.16×10^{-3} mW), same as [30], in which the antenna is operating at 0.915 GHz for data transmission. The local SAR distributions of the proposed antenna at 0.915 GHz within the previous tissue cylinder ($D_t \times D_p$, 110 mm × 80 mm) are shown in Fig. 10, which presents the distributions of both *xoz* and *yoz* planes. From the figure we can see that the local SAR concentrates on the top and along vertical sides of the capsule. The maximum SAR values at 0.915 GHz and 1.4 GHz are listed in Table 3. The SAR values at 1.4 GHz are lower, but its distributions are similar with that of 0.915 GHz, therefore not shown for brevity. From the table we can also notice that the maximum local SAR generated is 2.9×10^{-2} W/kg, well below the stipulated 2 W/kg over 10 grams of tissue according to IEEE Standard C95.1-2005 [29].

TABLE 3. Antenna's SAR values.

Frequency	0.915 GHz		1.4 GHz	
Distribution plane	*xoz*	*yoz*	*xoz*	*yoz*
SAR values (W/kg)	4.4e-3	2.9e-2	1.5e-3	1.4e-2

IV. COMMUNICATION LINK EVALUATION

A. COUPLING STRENGTH

For the evaluation of coupling strength, one common practice is to place an external antenna as receiver in proximity to the implanted antenna to evaluate the received power [3], [4], [11]. However, when the measurement is set up in this way, the coupling between the two connecting cables is inevitable, which sometimes is even stronger than the coupling between antennas. In order to minimize the effect of the connecting cables, a patch antenna with coaxial feeding at the bottom is chosen as the external antenna. Therefore the radiation of extending cable can be partially isolated by the patch antenna's large ground plane. In addition, the feeding

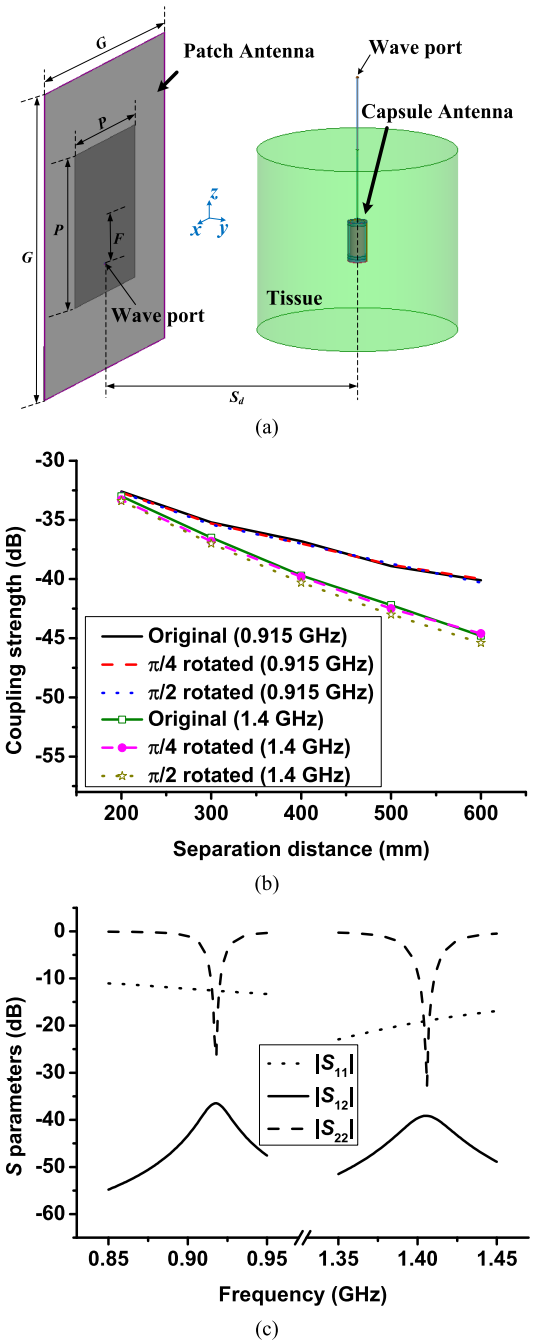

FIGURE 11. (a) Simulation setup of communication link. (b) Simulated coupling strength between internal capsule antenna and external patch antenna. (c) Simulated *S* parameters of the communication link at a separation distance of 400 mm.

TABLE 4. Patch antenna's geometric parameters and gain values.

Operating frequency	G (mm)	P (mm)	F (mm)	Gain (dBi)
0.915 GHz	170	84.8	26	-0.2
1.4 GHz	110	55.3	13.5	1.7

cables of receiver and implanted antenna are set perpendicular to each other to minimize their interaction. The simulation setup is shown in Fig. 11(a), in which the capsule antenna is positioned in the geometric center of the tissue cylinder. The feeding port for the external antenna is located right below the patch antenna's ground, while the feeding port for the implanted antenna is located above the coaxial cable. Such a setup for simulation can be easily implemented in experiment and be better compared with measurement, where the reference plane for calibration is set correspondingly.

For the external patch antenna, two antennas operating at 0.915 GHz and 1.4 GHz are used, which are fabricated on Rogers 4350B with a thickness of 0.508 mm. The two antenna's geometric parameters and gain values are shown in Table 4, where F is the distance between the feeding point and the patch's geometric center. For the capsule antenna, three orientations are chosen. The first one is positioned with its original x-axis in Fig. 2 set perpendicular to the patch antenna's surface. The other two orientations are positioned with the capsule rotated along z-axis by $\pi/4$ and $\pi/2$ respectively. For the separation distance between two antennas, S_{d} is varied from 200 to 600 mm at a step of 100 mm, and the comparison of antennas' coupling strength at two desired bands and three orientations are shown in Fig. 11(b). From Fig. 11(b) we can see that as the separation distance increases, the coupling strength gradually reduces, which is around $-33 \sim -40$ dB at 0.915 GHz and $-33 \sim -45$ dB at 1.4 GHz. The coupling at 1.4 GHz is lower than that at 0.915 GHz due to larger absorption by tissue at higher frequency. Therefore, for actual application we can use 1.4 GHz WMTS band to generate a startup signal to wake up the capsule device and use 0.915 GHz ISM band for data transfer. In addition, we notice that the coupling difference between three orientations is quite small, with a slightly larger difference at WMTS band (still within 0.8 dB for all separation distances). As an example, the S parameters of the two port system at a distance of 400 mm are shown in Fig. 11(c), where port 1 represents the internal capsule antenna and port 2 represents the external patch antenna.

B. LINK BUDGET

The analysis of link budget has been presented in [26]. Therefore, we only give a brief calculation of the link margin in this work. The parameters used in calculation are listed in Table 5. All values are set the same as [26] except that the input power (-25 dBm) is from [30], which is kept the same as used in Section III for SAR evaluation. The link margin (LM) can be calculated by [26]

$$LM = P_T - PL - RNF - IL - SNR \tag{2}$$

TABLE 5. Link budget.

Operating frequency	0.915 GHz
Transmitter Power (P_{T})	-25 dBm
Distance	0.2~0.6 m
Path Loss (PL)	33~40 dB
Implementation Loss (IL)	6 dB
Receiver Noise Floor (RNF)	-101 dBm
Signal to Noise Ratio (SNR)	14 dB

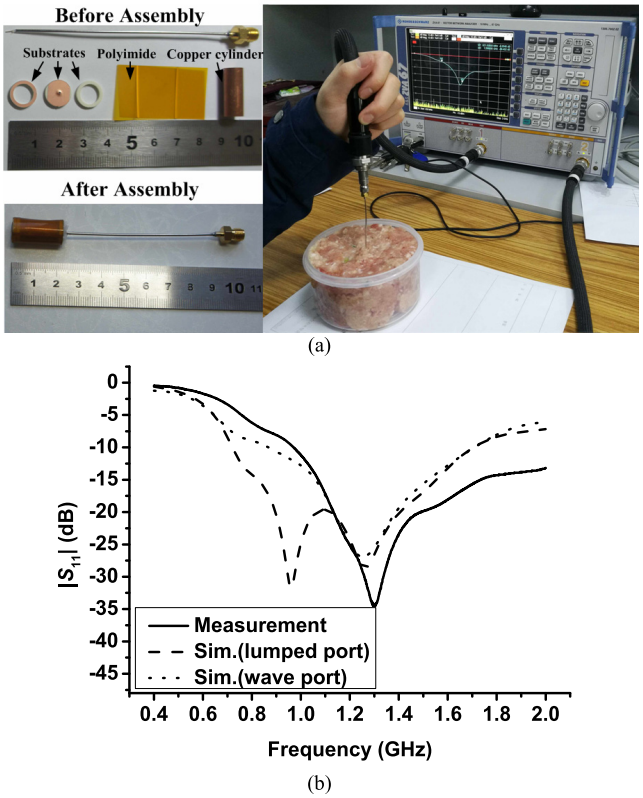

FIGURE 12. (a) Fabricated antenna and measurement setup. (b) Comparison of measured reflection coefficient with simulated one.

which is 16~23 dB as calculated according to Table 5. This link margin is obtained under the condition of a stringent bit rate error (BER) of 1×10^{-5}. If the system requirement is less demanding, the link margin can be improved further. Also, even if the EM wave generated by the capsule antenna propagates through a thicker tissue, the margin is still big enough to compensate higher loss.

V. ANTENNA MEASUREMENT

The fabricated antenna is composed of three Rogers 4350B substrates, a copper cylinder, a thin layer of foam, one polyimide substrate with two copper strip parts and another polyimide substrate intended to be loaded on top. The separate components before assembly together with assembled antenna are shown in Fig. 12(a). The coaxial cable's length is 100 mm, which is soldered to the antenna, and then the whole device is inserted into minced pork for measurement. The measurement is performed by vector network analyzer

TABLE 6. Performance comparison of proposed antenna with past works.

Ref.	Caps. size (D × L_g)	Tissue Size (mm^3)	Frequency	Bandwidth	Gain (dBi)	Efficiency	Radiation
[3]	10.5 mm × 20.0 mm	$\pi \times 150^2 \times$ unknown	430 ~ 500 MHz	70 MHz	N/A	N/A	Isotropic
[5]	8.5 mm × 23.3 mm	human model	611, 915, 2442 MHz	N/A	N/A	N/A	N/A
[6]	11.0 mm × 26.0 mm	human model	1.4 GHz	Appr. 150 MHz	-26.1	0.05 %	Directional
[9]	11.0 mm × 24.0 mm	$\pi \times 150^2 \times$ unknown	370 ~ 630 MHz	260 MHz	N/A	N/A	Omnidirectional
[11]	11.0 mm × 26.0 mm	100 × 100 × 100 (1×10^6)	2.4 ~ 2.48 GHz	816 MHz (AR)	-32.0	N/A	Directional
[12]	11.0 mm × 26.0 mm	100 × 100 × 100 (1×10^6)	915 MHz	267 MHz (AR)	-19.4	N/A	Directional
[15]	10.0 mm × 18.5 mm	human model	433 MHz	N/A	around -25	1.9 %	Omnidirectional
Ours	11.0 mm × 22.0 mm	$\pi \times 55^2 \times 80$ (7.6×10^5)	721 ~ 1705 MHz	984MHz	-13.0 ISM	1.14 %	Omnidirectional
					-16.1 WMTS	0.09 %	Omnidirectional
		$\pi \times 110^2 \times 160$ (6.1×10^6)	732 ~ 1699 MHz	967 MHz	-28.2 ISM	0.11 %	Omnidirectional
					-29.4 WMTS	0.04 %	Omnidirectional

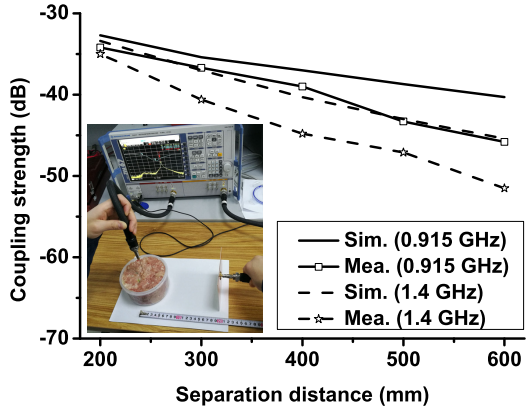

FIGURE 13. Measurement setup of communication link and the comparison of measured coupling strength with simulated one.

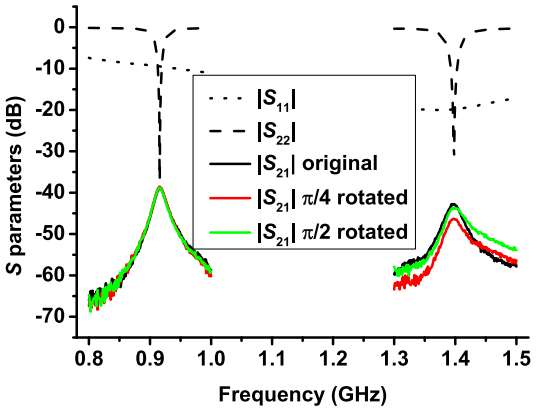

FIGURE 14. Measured *S* parameters at three different orientations with a link separation distance of 400 mm.

Rhode & Schwarz ZVA 67, and the measurement setup is also shown in Fig. 12(a). The comparison between measurement result and simulated one is presented in Fig. 12(b). It is noticed that the measurement result agrees well with simulated one, especially with the case fed by wave port. However, we should keep in mind that the lumped port case with a wider bandwidth is closer to actual application.

The measurement setup for coupling strength and the result comparison with simulated one at both 0.915 GHz and 1.4 GHz are shown in Fig. 13. It is noticed that the measured result is smaller than simulated one, which is caused by factors such as reduced matching performance and misalignment.

In addition, as the antenna is symmetric with respect to both *xoz* and *yoz* planes, we evaluate the link with the implanted antenna oriented in three typical directions. One is positioned with its original x-axis set perpendicular to the patch antenna's surface as in Subsection A of Section IV, and then the capsule antenna is rotated around the feeding cable by $\pi/4$ and $\pi/2$. Fig. 14 shows the measured S parameters at three different orientations with a link separation distance of 400 mm, which reveals that the antenna can maintain a consistent coupling strength with external antenna, especially at 0.915 GHz ISM band. The measured results further validate the proposed antenna's omnidirectional radiation capability at its azimuthal plane.

VI. CONCLUSION

In this paper, a wireless capsule antenna is proposed for GI tract diagnosis. Firstly, based on a simplified schematic of WCE system, a novel antenna is proposed with the optic dome substituted by foam and electronic components housed in a copper cylinder. This enables the harmful EMI generated by battery, sensors and other electronic components to be reduced to the minimum. Secondly, the operating principle of antenna is explained by discussing the effects of foam thickness, followed with antenna simulation for robustness evaluation, radiation pattern, and the effects of tissue size and feeding cable. For safety reason concerning human body's exposure to EM wave, local SAR distributions are also evaluated. Furthermore, the communication link is evaluated, with the link margin calculated to ensure the system's reliability. Finally, the measurement in minced pork is performed for validation of simulation results.

The proposed antenna's performance comparison with past research works is summarized in Table 6. It can be seen that the proposed antenna can achieve a decent gain with wide bandwidth while maintaining an omnidirectional radiation pattern across all operating frequencies.

In conclusion, the proposed antenna successfully utilizes the entire aperture of the capsule, which helps maximize

the gain bandwidth product. Furthermore, a central copper cylinder is introduced to house the transmitter circuits and battery, which not only minimizes the EMI but also helps boost the radiation performance. Thirdly, the antenna uses copper strip with stepped width to tune the matching, leading to a very wide bandwidth of 984 MHz (81.1 %), making the antenna robust enough against diversified human tissues. Finally, due to strong electric field concentrated within the top substrate, the proposed antenna can maintain an omnidirectional radiation pattern across all frequencies, which is a very advantageous characteristic due to the capsule's unknown orientation in GI tract. The proposed antenna's advantages listed above make it a promising candidate of GI tract diagnosis intended for human health.

REFERENCES

[1] M. R. Yuce and T. Dissanayake, "Easy-to-swallow wireless telemetry," *IEEE Microw. Mag.*, vol. 13, no. 6, pp. 90–101, Sep. 2012.

[2] M. R. Yuce and T. Dissanayake, "Easy-to-swallow antenna and propagation," *IEEE Microw. Mag.*, vol. 14, no. 4, pp. 74–82, Jun. 2013.

[3] S. I. Kwak, K. Chang, and Y. J. Yoon, "Small spiral antenna for wideband capsule endoscope system," *Electron. Lett.*, vol. 42, no. 23, pp. 1328–1329, Nov. 2006.

[4] S. H. Lee *et al.*, "A wideband spiral antenna for ingestible capsule endoscope systems: Experimental results in a human phantom and a pig," *IEEE Trans. Biomed. Eng.*, vol. 58, no. 6, pp. 1734–1741, Jun. 2011.

[5] H. Yu *et al.*, "Printed capsule antenna for medication compliance monitoring," *Electron. Lett.*, vol. 43, no. 22, pp. 1170–1181, Oct. 2007.

[6] P. M. Izdebski, H. Rajagopalan, and Y. Rahmat-Samii, "Conformal ingestible capsule antenna: A novel chandelier meandered design," *IEEE Trans. Antennas Propag.*, vol. 57, no. 4, pp. 900–909, Apr. 2009.

[7] H. Rajagopalan and Y. Rahmat-Samii, "Wireless medical telemetry characterization for ingestible capsule antenna designs," *IEEE Antennas Wireless Propag. Lett.*, vol. 11, pp. 1679–1682, Jan. 2013.

[8] D. Nikolayev, M. Zhadobov, L. L. Coq, P. Karban, and R. Sauleau, "Robust ultraminiature capsule antenna for ingestible and implantable applications," *IEEE Trans. Antennas Propag.*, vol. 65, no. 11, pp. 6107–6119, Nov. 2017.

[9] S. Yun, K. Kim, and S. Nam, "Outer-wall loop antenna for ultrawideband capsule endoscope system," *IEEE Antennas Wireless Propag. Lett.*, vol. 9, pp. 1135–1138, 2010.

[10] M. M. Suzan, K. Haneda, C. Icheln, A. Khatun, and K.-I. Takizawa, "An ultrawideband conformal loop antenna for ingestible capsule endoscope system," in *Proc. 10th Eur. Conf. Antennas Propag. (EuCAP)*, Apr. 2016, pp. 1–5.

[11] C. Liu, Y.-X. Guo, and S. Xiao, "Circularly polarized helical antenna for ISM-band ingestible capsule endoscope systems," *IEEE Trans. Antennas Propag.*, vol. 62, no. 12, pp. 6027–6039, Dec. 2014.

[12] R. Das and H. Yoo, "A wideband circularly polarized conformal endoscopic antenna system for high-speed data transfer," *IEEE Trans. Antennas Propag.*, vol. 65, no. 6, pp. 2816–2826, Jun. 2017.

[13] Y. Li, Y.-X. Guo, and S. Q. Xiao, "Orientation insensitive antenna with polarization diversity for wireless capsule endoscope system," *IEEE Trans. Antennas Propag.*, vol. 65, no. 7, pp. 3738–3743, Jul. 2017.

[14] Z. Duan and L.-J. Xu, "Dual-band implantable antenna with circular polarisation property for ingestible capsule application," *Electron. Lett.*, vol. 53, no. 16, pp. 1090–1092, Aug. 2017.

[15] X. Cheng, J. Wu, R. Blank, D. E. Senior, and Y.-K. Yoon, "An omnidirectional wrappable compact patch antenna for wireless endoscope applications," *IEEE Antennas Wireless Propag. Lett.*, vol. 11, pp. 1667–1670, 2012.

[16] X. Cheng, D. E. Senior, C. Kim, and Y.-K. Yoon, "A compact omnidirectional self-packaged patch antenna with complementary split-ring resonator loading for wireless endoscope applications," *IEEE Antennas Wireless Propag. Lett.*, vol. 10, pp. 1532–1535, 2011.

[17] W. Geyi, "Physical limitations of antenna," *IEEE Trans. Antennas Propag.*, vol. 51, no. 8, pp. 2116–2123, Aug. 2003.

[18] W. Geyi, "A new derivation of the upper bounds for the ratio of gain to Q," *IEEE Trans. Antennas Propag.*, vol. 60, no. 7, pp. 3488–3490, Jul. 2012.

[19] W. Geyi, "Optimization of the ratio of gain to *Q*," *IEEE Trans. Antennas Propag.*, vol. 61, no. 4, pp. 1916–1922, Apr. 2013.

[20] F. Merli, B. Fuchs, J. R. Mosig, and A. K. Skrivervik, "The effect of insulating layers on the performance of implanted antennas," *IEEE Trans. Antennas Propag.*, vol. 59, no. 1, pp. 21–31, Jan. 2011.

[21] Z. Duan, L.-J. Xu, and G. Wen, "Metal frame repeater antenna with partial slotted ground for bandwidth enhancement of wristband devices," *IET Microw. Antennas Propag.*, vol. 11, no. 10, pp. 1438–1444, Jul. 2017.

[22] L.-J. Xu and Z. Duan, "Differential wide band metal-frame antenna for wristband applications," in *Proc. IEEE MTT-S Int. Microw. Workshop Ser. Adv. Mater. Process. RF THz Appl. (IMWS-AMP)*, Chengdu, China, Jul. 2016, pp. 1–3.

[23] Z. Duan and L.-J. Xu, "Dual band wristband antenna with metal frame loaded for biomedical applications," *Microw. Opt. Technol. Lett.*, vol. 59, no. 9, pp. 2155–2159, Sep. 2017.

[24] A. Kiourti, J. R. Costa, C. A. Fernandes, and K. S. Nikita, "A broadband implantable and a dual-band on-body repeater antenna: Design and transmission performance," *IEEE Trans. Antennas Propag.*, vol. 62, no. 6, pp. 2899–2908, Jun. 2014.

[25] S. Gabriel, R. W. Lau, and C. Gabriel, "The dielectric properties of biological tissues: III. Parametric models for the dielectric spectrum of tissues," *Phys. Med. Biol.*, vol. 41, no. 11, pp. 2231–2293, Nov. 1996.

[26] Z. Duan, Y.-X. Guo, R.-F. Xue, M. Je, and D.-L. Kwong, "Differentially fed dual-band implantable antenna for biomedical applications," *IEEE Trans. Antennas Propag.*, vol. 60, no. 12, pp. 5587–5595, Dec. 2012.

[27] Z. Duan, Y.-X. Guo, M. Je, and D.-L. Kwong, "Design and in vitro test of a differentially fed dual-band implantable antenna operating at MICS and ISM bands," *IEEE Trans. Antennas Propag.*, vol. 62, no. 5, pp. 2430–2439, May 2014.

[28] F. Merli, L. Bolomey, J.-F. Zurcher, G. Corradini, E. Meurville, and A. K. Skrivervik, "Design, realization and measurements of a miniature antenna for implantable wireless communication systems," *IEEE Trans. Antennas Propag.*, vol. 59, no. 10, pp. 3544–3555, Oct. 2011.

[29] *IEEE Standard for Safety Levels With Respect to Human Exposure to Radio Frequency Electromagnetic Fields, 3 kHz to 300 GHz*, IEEE Standard C95.1-2005, 2006.

[30] H. Yu, C.-M. Tang, and R. Bashirullah, "An asymmetric RF tagging IC for ingestible medication compliance capsules," in *Proc. IEEE Radio Freq. Integr. Circuits Symp.*, Jun. 2009, pp. 101–104.

ZHU DUAN (M'12) was born in Xianning, China, in 1987. He received the B.S. degree from the Department of Electronic Science and Technology, Huazhong University of Science and Technology, Wuhan, China, in 2009, and the Ph.D. degree from National University of Singapore in 2013. From 2014 to 2015, he was a Chief Engineer of antenna and feeding system with the East China Research Institute of Electronic Engineering. In 2015, he joined the School of Electronic and Information Engineering, Nanjing University of Information Science and Technology. His main research interests include implantable, wearable antennas and wireless power transfer for biomedical applications.

LI-JIE XU received the B.E. degree in optoelectronic information and engineering and the Ph.D. degree in electromagnetic field and microwave technology from Nanjing University of Science and Technology in 2009 and 2014, respectively. From 2010 to 2011, she was a Visiting Scholar with the Department of Electrical and Computer Engineering, National University of Singapore, where she was a Joint Ph.D. Student from 2011 to 2013, supported by China Scholarship Council. She has been a Lecturer with the College of Electronic and Optical Engineering, Nanjing University of Post and Telecommunications, since 2015, and a Post-Doctoral Researcher with the School of Information Science and Engineering, Southeast University, since 2017. Her main research interests include implantable/wearable antennas for biomedical applications and low-pass and band-pass filters.

STEVEN GAO (M'01–SM'16) received the Ph.D. degree in microwave engineering from Shanghai University, Shanghai, China, in 1999. He is currently the Chair of RF and microwave engineering and the Director of Postgradudate Research with the School of Engineering and Digital Arts, University of Kent, U.K. He has co-authored/co-edited two books and over 300 papers in international journals and conferences, and holds four patents. His main areas of expertise are in antennas, smart antennas, phased arrays, multi-in multi-out, satellite antenna, RF/microwave/millimetre-wave/terahertz circuits and RF front ends, 5G mobile communications, satellite communications, wireless power transfer, UWB radars, GNSS reflectometry, synthetic-aperture radars, electromagnetic modeling, and small satellites.

He is a member of the editorial boards of the *International Journal of Space Science and Engineering*, USA, the *IET Circuits, Devices &Systems*, U.K., the *Chinese Journal of Electronics*, China, and the *Chinese Journal of Radio Science*, China. He received the 2016 IET Premium Award for the Best Paper in IET Microwave, Antennas and Propagation and the 2017 CST University Publication Award for a paper in the IEEE Transactions on Antennas and Propagation. He is an Associate Editor of the IEEE Transactions on Antennas and Propagation, the *Radio Science*, and the IEEE Access and the Editor-in-Chief of Wiley Book Series on "Microwave and Wireless Technologies." He was a Distinguished Lecturer of the IEEE Antennas and Propagation Society from 2014 to 2016, the General Chair of the 2013 Loughborough Antenna and Propagation Conference, a Leader Guest Editor of the IEEE Transactions on Antennas and Propagation for Special Issue on "Antennas for Satellite Communication" in 2015, a Guest Editor of the *IET Circuits, Devices & Systems* for Special Issue on "Photonic and RF Communications Systems" in 2014, the Chair of Special Session on "Satellite Communication Antennas" in CSNDSP'2012, and the Chair of Workshop on "New Technology Development for Space" in 2015 IEEE Microwave Symposium. He was a Plenary/Invited Speaker of some international conferences and workshops (IEEE APWC'2017, UCMMT'2017, AES'2014, IWAT'2014, SOMIRES'2013, and APCAP'2014). He is a Fellow of IET, U.K., and the Royal Aeronautical Society, U.K.

WEN GEYI (M'88) was born in Pingjiang, Hunan, China, in 1963. He received the B.Eng., M.Eng., and Ph.D. degrees in electrical engineering from Xidian University, China, in 1982, 1984, and 1987, respectively.

He was a Lecturer with the Radio Engineering Department, Southeast University, from 1988 to 1990; an Associate Professor with the Institute of Applied Physics, University of Electronic Science and Technology of China (UESTC), from 1990 to 1992; a Visiting Researcher with the Department of Electrical and Computer Engineering, University of California at Berkeley, from 1992 to 1993; and a Full Professor with the Institute of Applied Physics, UESTC, from 1993 to 1998. From 1996 to 1997, he was the Vice Chairman of the Institute of Applied Physics, UESTC, where he was also the Chairman from 1997 to 1998. In 1998, he joined the Electrical Engineering Department, University of Waterloo, as a Visiting Professor. From 1998 to 2007, he was with Blackberry Ltd., Canada, first as a Senior Scientist with the Radio Frequency Department and then the Director of the Advanced Technology Department. Since 2010, he has been a National Distinguished Professor of China first with Fudan University, Shanghai, and then with the Nanjing University of Information Science and Technology (NUIST), Nanjing, China. He is currently the Director of the Research Center of Applied Electromagnetics, NUIST. He has authored or co-authored over 100 journal publications. He has authored the *Foundations for Radio Frequency Engineering* (World Scientific, 2015), the *Foundations of Applied Electrodynamics* (Wiley, 2010), the *Advanced Electromagnetic Field Theory* (National Defense Publishing House, 1999), in Chinese, and the *Modern Methods for Electromagnetic Computations* (Henan Science and Technology Press, 1994), in Chinese. He holds over 40 invention patents. His current research interests include microwave theory and techniques and antennas and wave propagation.